Failure to Maintain Acetate Homeostasis by Acetate-Activating Enzymes Impacts Plant Development[1][OPEN]

Xinyu Fu,[a,b,c] Hannah Yang,[a] Febriana Pangestu,[a] and Basil J. Nikolau[a,b,c,2,3]

[a]Department of Biochemistry, Biophysics, and Molecular Biology, Iowa State University, Ames, Iowa 50011
[b]Center for Biorenewable Chemicals (CBiRC), Iowa State University, Ames, Iowa 50011
[c]Center for Metabolic Biology, Iowa State University, Ames, Iowa 50011

ORCID IDs: 0000-0003-4178-238X (X.F.); 0000-0002-4672-7139 (B.J.N.).

The metabolic intermediate acetyl-CoA links anabolic and catabolic processes and coordinates metabolism with cellular signaling by influencing protein acetylation. In this study we demonstrate that in Arabidopsis (*Arabidopsis thaliana*), two distinctly localized acetate-activating enzymes, ACETYL-COA SYNTHETASE (ACS) in plastids and ACETATE NON-UTILIZING1 (ACN1) in peroxisomes, function redundantly to prevent the accumulation of excess acetate. In contrast to the near wild-type morphological and metabolic phenotypes of *acs* or *acn1* mutants, the *acs acn1* double mutant is delayed in growth and sterile, which is associated with hyperaccumulation of cellular acetate and decreased accumulation of acetyl-CoA-derived intermediates of central metabolism. Using multiple mutant stocks and stable isotope-assisted metabolic analyses, we demonstrate the twin metabolic origins of acetate from the oxidation of ethanol and the nonoxidative decarboxylation of pyruvate, with acetaldehyde being the common intermediate precursor of acetate. Conversion from pyruvate to acetate is activated under hypoxic conditions, and ACS recovers carbon that would otherwise be lost from the plant as ethanol. Plastid-localized ACS metabolizes cellular acetate and contributes to the de novo biosynthesis of fatty acids and Leu; peroxisome-localized ACN1 enables the incorporation of acetate into organic acids and amino acids. Thus, the activation of acetate in distinct subcellular compartments provides plants with the metabolic flexibility to maintain physiological levels of acetate and a metabolic mechanism for the recovery of carbon that would otherwise be lost as ethanol, for example following hypoxia.

Acetyl-CoA is a metabolic intermediate juxtaposed between anabolic and catabolic processes (Oliver et al., 2009; Pietrocola et al., 2015). Anabolic processes include the biosynthesis of energy-dense biochemicals (i.e. fatty acids, hydrocarbons, and terpenes) and many bioactive compounds (e.g. polyketides and flavonoids). As an acetyl-group donor, acetyl-CoA also plays a role as a "sentinel" molecule that links metabolism with cellular signaling by influencing the prevalence of protein acetylation modifications (Wu et al., 2011; Galdieri et al., 2014). Catabolic processes that generate acetyl-CoA include β-oxidation of fatty acids (Graham, 2008) and catabolism of acetogenic amino acids (e.g. Leu; Hildebrandt et al., 2015). Because the structure and dynamics of the acetyl-CoA metabolic network are highly compartmentalized in eukaryotic organisms, it is far from being fully understood (Oliver et al., 2009; Krivoruchko et al., 2015). Therefore, to better exploit the metabolic diversity and flexibility of plants, there is a need to better understand how acetyl-CoA generation and utilization are genetically and biochemically coordinated among different cellular and subcellular compartments in the context of the broader metabolic and genetic networks.

Due to the impermeability of membranes to acetyl-CoA, this key intermediate is independently generated and metabolized in distinct subcellular compartments (Oliver et al., 2009; Schwender and Ohlrogge, 2002). The first acetyl-CoA-generating enzyme to be characterized in plants was acetyl-CoA synthetase (ACS), which activates acetate to its CoA-ester (Huang and Stumpf, 1970). ACS was implicated as the dominant source of acetyl-CoA for fatty acid biosynthesis because [^{14}C]acetate is efficiently incorporated into fatty acids by isolated chloroplasts (Roughan et al., 1979).

[1]This work was partly supported by the U.S. Department of Energy (DOE) (award no. 0000217546), Office of Basic Energy Sciences, Division of Chemical Sciences and the National Science Foundation Engineering Research Center for Biorenewable Chemicals (CBiRC; http://www.cbirc.iastate.edu; NSF award EEC 0813570).

[2]Author for contact: dimmas@iastate.edu.
[3]Senior author.
The author responsible for distribution of materials integral to the findings presented in this article in accordance with the policy described in the Instructions for Authors (www.plantphysiol.org) is: Basil J. Nikolau (dimmas@iastate.edu).

B.J.N. and X.F. conceived the research plans; X.F. performed the experiments and analyzed the data; H.Y. and F.P. provided technical assistance to X.F.; B.J.N. and X.F. wrote the article.
[OPEN]Articles can be viewed without a subscription.
www.plantphysiol.org/cgi/doi/10.1104/pp.19.01162

The identification of a plastidic pyruvate dehydrogenase complex (ptPDHC; Williams and Randall, 1979) and the rapid in vivo incorporation of label from carbon dioxide into fatty acids (Bao et al., 2000) suggest that plastidic acetyl-CoA is generated from pyruvate derived from photosynthesis. Reverse genetic characterizations of ptPDHC and ACS established the importance of the former, whereas mutations in the latter minimally affect fatty acid biosynthesis and normal plant growth (Lin et al., 2003).

Several other acetyl-CoA-generating enzymes/pathways have been identified as essential to plant survival. These include ATP-citrate lyase (ACL), which generates the cytosolic acetyl-CoA pool (Fatland et al., 2002; Fatland et al., 2005); the mitochondrial isozyme of pyruvate dehydrogenase complex (mtPDHC), which generates the mitochondrial acetyl-CoA pool (Yu et al., 2012); and the fatty acid β-oxidation cycle, which generates the peroxisomal acetyl-CoA pool (Graham, 2008).

The Arabidopsis (*Arabidopsis thaliana*) genome encodes a large number of acyl-activating enzymes (the AAE superfamily) that activate carboxylates through the intermediate, acyl-AMP (EC 6.2.1; Shockey et al., 2003; Shockey and Browse, 2011). Two of these, ACS and ACETATE NON-UTILIZING1 (ACN1; Hooks et al., 2004; Turner et al., 2005), are distantly related members of this superfamily, and both preferentially activate acetate to generate acetyl-CoA (Turner, et al., 2005; Lin and Oliver, 2008; Sofeo et al., 2019). ACS is plastid-localized (Kuhn et al., 1981), whereas ACN1 is localized in peroxisomes (Turner, et al., 2005). These characterizations raise questions regarding the role of compartment-specific acetyl-CoA generation from acetate in plastids and peroxisomes of plant cells. Integrated with that question is the limited knowledge concerning the endogenous origin of the acetate substrate (Liedvogel and Stumpf, 1982; Bao et al., 2000).

The aim of this study was to characterize the functions and interplay of ACS and ACN1 in compartment-specific acetate/acetyl-CoA metabolism in Arabidopsis. A combination of stable isotope labeling studies and metabolomics analysis in the context of genetic mutants demonstrates that the plastidic ACS and peroxisomal ACN1 provide redundant functions to prevent hyper-accumulation of acetate, which affects normal growth, development, and central metabolism.

RESULTS

Characterization of *acs* and *acn1* Mutants

The physiological roles of the *ACS* and *ACN1* genes were explored by characterizing plants that carry Transfer DNA (T-DNA)-tagged mutant alleles at each locus, and plants that simultaneously carry these two mutations (Supplemental Fig. S1A). Reverse-transcription PCR (RT-PCR) analysis of RNA isolated from wild-type (ecotype Columbia of Arabidopsis [Col-0]) and mutant plants confirmed that each mutant line carries a null allele, and that mutations in the *ACS* gene do not affect *ACN1* expression and, vice versa, mutations in the *ACN1* gene do not affect *ACS* expression (Supplemental Fig. S1B).

Phenotypically, the individual *acs* or *acn1* homozygous mutants did not exhibit any discernable defects in growth and development, with normal root growth and elongation, rosette expansion, time to flowering, and stem elongation (Fig. 1; Supplemental Table S1). By contrast, all homozygous double mutant plants showed highly pleiotropic defects with extremely delayed vegetative and reproductive growth and development (Figs. 1 and 2A). χ^2 statistical tests confirmed the linkage between the abnormal phenotype and the simultaneous homozygosity for the recessive mutant alleles at the two unlinked genes (Supplemental Table S2). Because the four double mutant lines that were evaluated (i.e. *acs-1 acn1-4*, *acs-1 acn1-5*, *acs-2 acn1-4*, and *acs-2 acn1-5*) consistently exhibited near-identical phenotypes, detailed data are presented only from the *acs-1 acn1-5* double mutant line as representative of the double mutants. Therefore, the conclusions described below robustly establish that the simultaneous loss of both ACS and ACN1 functions is associated with many growth defect phenotypes.

Homozygous *acs-1 acn1-5* double mutant plants did not develop normally (Fig. 2A) and were ultimately infertile. Therefore, for characterization purposes, double mutant homozygous plants were identified from the progeny of sesquimutant parents, namely plants that are homozygous mutant at either the *acs* or *acn1* locus and heterozygous at the other locus. As with the single mutants, each of these sesquimutant lines (i.e. *acs-1/acs-1 acn1-5/ACN1-5* and *acs-1/ACS-1 acn1-5/acn1-5*) displayed a normal, wild type-like morphological phenotype, and the selfed progeny segregated the heterozygous allele with the expected 1:2:1 Mendelian ratio for a recessive allele (Supplemental Table S3). Therefore, gamete formation, fertilization, embryogenesis, and seed development are unaffected in the presence of at least one functional *ACS* or *ACN1* wild-type allele.

The first visible trait that differentiated double-mutant plants from single-mutant, sesquimutant, or wild-type plants was the delayed expansion of the first pair of leaves (Supplemental Fig. S2); in our growth conditions this process was delayed by 6 d in the double mutant. Additional phenotypes became increasingly apparent as these plants aged. These aberrations manifested slower root elongation and rosette expansion (Supplemental Table S1). Furthermore, rosette leaves exhibited an altered morphology, marked by an irregular shape, short petioles, serrated margins, and curled edges (Fig. 2A). The transition from vegetative to reproductive phases (time to bolting and flowering) was substantially delayed in the double mutants; these plants bolted 32 d after the wild type (Supplemental Table S1), after they had produced at least 30–50 leaves, whereas wild-type plants bolted after producing 8–10 leaves. Moreover, the double mutants showed reduced apical

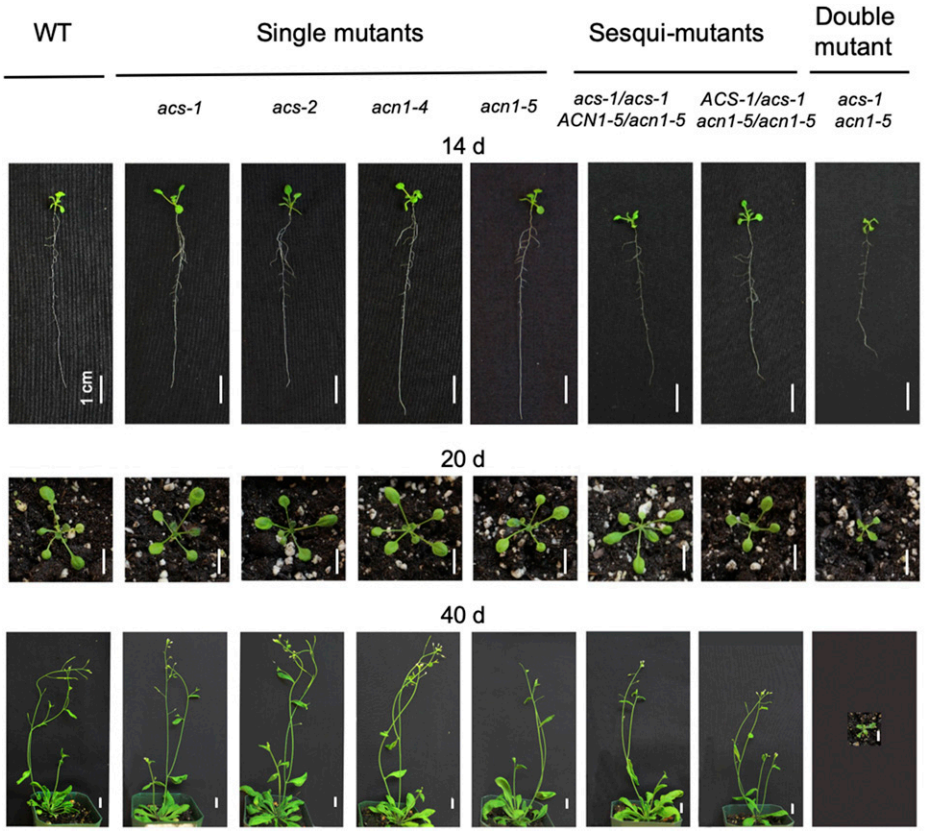

Figure 1. Vegetative and reproductive growth of *acs* and *acn1* single mutants, *acs-1 acn1-5* sesqui-mutants, and *acs-1 acn1-5* double mutants. Images of the wild type (WT) alongside the indicated mutant genotypes were captured at defined growth periods (days [d]) after planting. All plants were simultaneously grown in adjoining positions in a growth room under continuous illumination. Statistical analysis of the root length, rosette diameter, height of mature bolt, and time to floral transition of these mutants are shown in Supplemental Table S1.

dominance, which led to the "bushy appearance" of these plants. Additionally, the double mutants exhibited significantly delayed leaf senescence, and thus these plants remained green for up to 150 d, whereas wild-type plants had senesced by 90 d (Fig. 2A). The resulting dwarf-like phenotype of the double mutant resulted in a final bolt height that was only 10% of the wild-type height (Supplemental Table S1).

The infertility of the *acs-1 acn1-5* double mutants was shown to be due to aberrant flower inflorescences (Fig. 2B) and defects in floral development (Fig. 2C). Compared to the wild-type flowers, the flowers of the double mutants were smaller, with smaller anthers, shorter filaments, and malformed pistils, and no pollen was released from the anthers (Fig. 2D).

Alterations in Central Metabolism

The in planta metabolic consequence of eliminating the ACS and/or ACN1 function(s) was explored by profiling the metabolomes of the shoot and root tissues of wild-type, *acs-1* and *acn1-5* single-mutant, and *acs-1 acn1-5* double-mutant seedlings grown for 16 d on a defined medium. A total of 51 metabolites of central metabolism were identified, including 14 amino acids, 9 organic acids, 4 sugars, 3 phosphorylated intermediates, 3 amines, and 17 lipids. The volcano plots shown in Figure 3 identify those metabolites that were differentially accumulated in the mutant tissues with respect to the wild-type tissues. Consistent with the silent phenotypic nature of the *acs-1* and *acn1-5* single mutants, there were very few statistically significant differences in the metabolomes of either of these mutants. The most significant differences were associated with the roots of *acn1-5* mutant plants; levels of seven metabolites were decreased, with the greatest alteration a 40% reduction in Fru and Glc-6-phosphate levels (Supplemental Dataset S1). Similar but more substantial decreases in the levels of sugars, organic acids, and amino acids have previously been reported in such a mutant (Allen et al., 2011). The somewhat subtle differences between this study and Allen et al. (2011) may be associated with the fact that they gathered metabolic profiles from principal growth stage 0.7 (Boyes et al., 2001), using an *acn1-2* mutant allele that is in the Col-7 ecotype background (Nottingham Arabidopsis Stock Centre stock N21343 or Arabidopsis Biological Resource Center [ABRC] stock CS21343). The data in the current study were generated from older seedlings (principal growth stage 1.06), using the *acn1-5* allele that is in the Col-0 ecotype background (ABRC stock CS903402).

In contrast to the single mutants, the *acs-1 acn1-5* double mutant exhibited profound and distinct alterations in the metabolomes of shoots and roots. In shoots, the levels of 24 metabolites differed significantly from the wild type (8 increased and 16 decreased), and in roots, the levels of 43 metabolites were significantly reduced compared to the wild type (Fig. 3; Supplemental

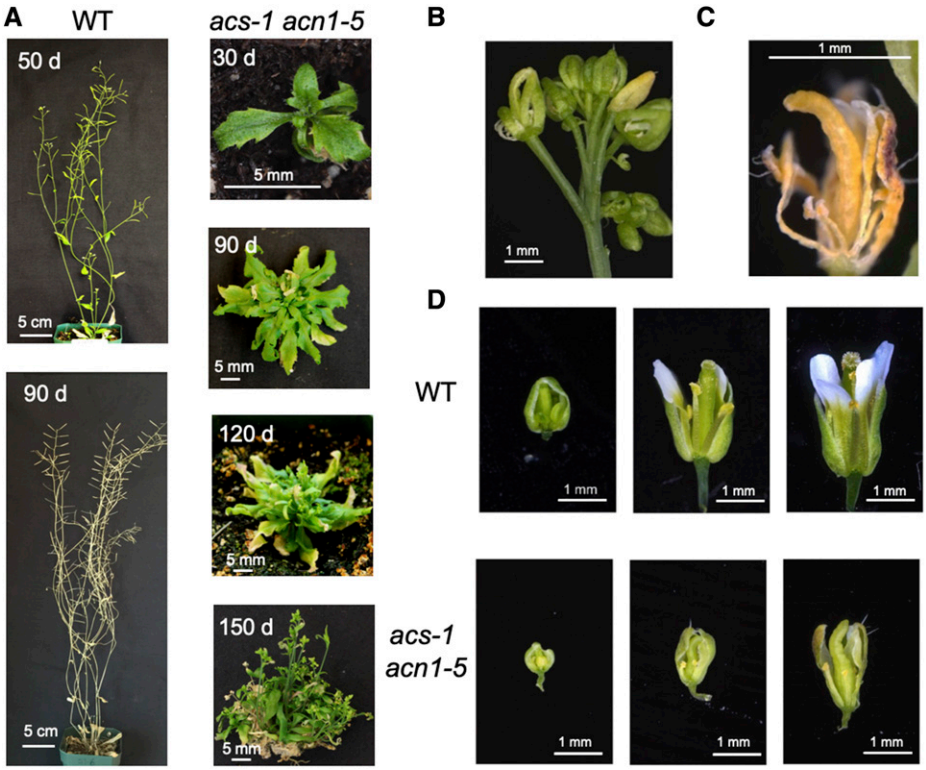

Figure 2. Phenotypic characterization of the *acs-1 acn1-5* double mutant plants. A, Wild-type (WT) and *acs-1 acn1-5* double mutant plants imaged at the indicated intervals after planting. The altered phenotypes include serrated leaf margins and short petioles (at 30 d); increased number of rosette leaves and delayed bolting (at 90 d); shorter and branched axillary inflorescences (at 120 d); and dwarfing and delayed senescence (at 150 d). B, Abnormal inflorescence architecture expressed by the *acs-1 acn1-5* double mutant. C, Magnified view of the defective floral structure of a senescing *acs-1 acn1-5* double mutant flower. D, Comparison of wild-type and *acs-1 acn1-5* double mutant flowers at the closed flower bud (left), half-open flower (middle), and open flower (right) stages. In each image, one sepal was removed to reveal the interior organs.

Dataset S1). Based on the number of metabolites that were altered in the two organs, we conclude that although the metabolic impact is similar in shoots and roots, the effect is more pronounced in the roots than in the shoots of seedlings. The specific metabolites that showed altered levels indicate that processes such as fatty acid metabolism and gluconeogenesis are affected by the *acs acn1* double mutation. These conclusions are based on the identification of the most dramatically altered metabolites: (1) Glc, Glc-6-phosphate, and Fru, which were decreased 5-fold from wild-type levels; (2) plastid-generated fatty acids (i.e. 14:0, 16:0, and 16:3) and endoplasmic reticulum-generated fatty acids (i.e. 20:0, 22:0, and 24:0) that were decreased between 2- and 5-fold; and (3) citrate and malate, which were decreased by ~5-fold (Supplemental Dataset S1).

Alterations in Acetate Metabolism

Consistent with the ability of both ACS and ACN1 to preferentially utilize acetate as the substrate to produce acetyl-CoA, compared to the wild-type seedlings, the in vivo concentration of acetate was about 2-fold higher in either of the *acs-1* or *acn1-5* single mutants and was further increased in the double mutant by ~10-fold, to reach 250 μmol g^{-1} dry weight (Fig. 4A). Based on these observations we hypothesized that the hyperaccumulation of acetate is causative of the growth phenotypes associated with the *acs-1 acn1-5* double mutant. We tested this hypothesis by growing wild-type plants on medium containing different concentrations of acetate (Fig. 4B). The inclusion of 1 mM acetate in the media resulted in inhibition of growth of both the shoots and roots, and increasing the concentration of acetate in the medium further increased the growth inhibition. Direct evaluation of these tissues confirmed that the exogenous acetate was taken up, resulting in increased acetate concentration in the tissue (Fig. 4A). Moreover, when the *acs-1* or *acn1-5* single mutants were grown on this medium, the growth inhibition by acetate was more pronounced than with the wild type, but not as pronounced as the *acs-1 acn1-5* double mutant (Figs. 4, C and D). Thus, the presence of a functional ACS or ACN1 is needed to metabolize acetate to acetyl-CoA and thus reduce the impact of acetate on plant growth. This growth inhibition caused by external acetate parallels the increased endogenous acetate levels in the plant tissue (Fig. 4A), and these results are consistent with prior observations of the toxicity of acetate to plant growth (Lin and Oliver, 2008; Turner et al., 2005).

Kinetics of ^{13}C Labeling of the Plastidic and Cytosolic Acetyl-CoA Pools

The flux though acetyl-CoA metabolism in plant cells was monitored by incubating seedlings with ^{13}C-labeled precursors (acetate or Glc). By comparing the kinetic labeling data obtained with *acs-1* or *acn1-5* mutants to the data obtained with wild-type plants, we could discriminate those processes that are dependent on plastidial ACS from those that are dependent on the peroxisomal ACN1.

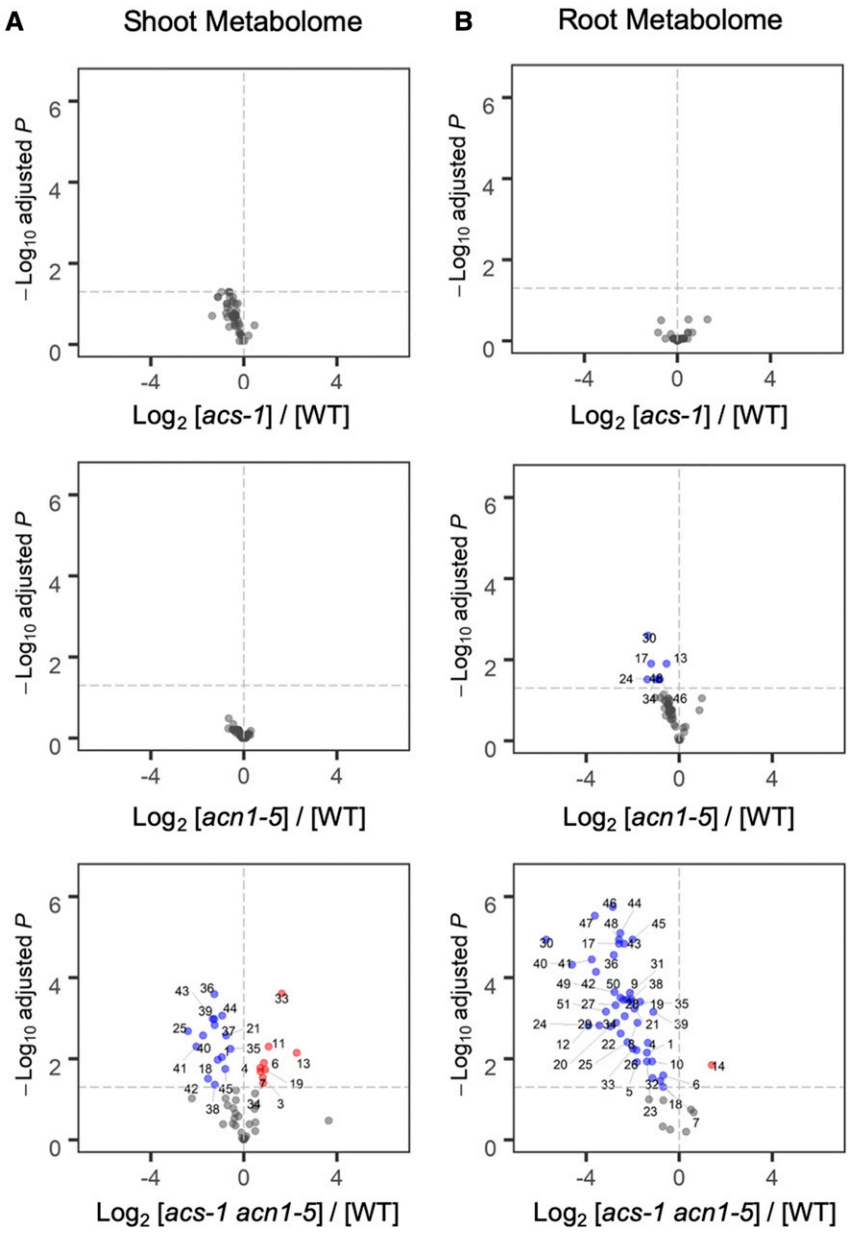

Figure 3. Metabolomic alterations in the *acs-1* and *acn1-5* single mutants and the *acs-1 acn1-5* double mutant. Volcano plot visualization of statistically significant changes in metabolite levels in the *acs-1* and *acn1-5* single mutant and *acs-1 acn1-5* double-mutant shoots (A) and roots (B), as compared to the levels in wild-type (WT) tissues. The *x* axis plots the log2-transformed relative ratio of the concentration (indicated by square brackets) of the metabolite in the mutant divided by the concentration of the metabolite in the wild type. The *y* axis represents the negative log of the Benjamini-Hochberg adjusted *P*-values. Red and blue data points above the horizontal dashed gray line indicate statistically significant ($P < 0.05$ [Benjamini-Hochberg adjusted], $n = 4$) changes in metabolites levels. The data points in each plot represent 51 metabolites identified in Supplemental Dataset S1, and these include amino acids (nos. 1–14), organic acids (nos. 15–23), sugars and sugar alcohols (nos. 24–27), phosphate and phosphorylated metabolites (nos. 28–31), amines (nos. 32–34), and lipids (nos. 35–51).

The labeling of plastidic and cytosolic acetyl-CoA was inferred by examining labeling of fatty acids, specifically the McLafferty mass spectrometry (MS) fragment ions (McLafferty, 1959) recovered from fatty acid methyl esters. The McLafferty fragment ion (i.e. *m/z* 74) is a typical fragment ion generated by the electron ionization that occurs during MS of these molecules, and this fragment contains the two carboxy-terminal carbon atoms of the fatty acid. Thus, the fractional abundance of the $[M + 2]^+$ ion of the McLafferty ion with a mass shift of 2 atomic mass units (i.e. *m/z* 76) represents the metabolic origins of the acetyl-CoA unit that was used in the final elongation cycle of the fatty acid synthase or fatty acid elongase reaction, which generates that fatty acid metabolite.

The contribution of ACS to the plastidic acetyl-CoA pool was revealed by analyzing the labeling of the McLafferty ion recovered from the methyl ester of hexadecanoic acid (16:0), which is a product of de novo fatty acid synthesis in plastids (Fig. 5A). Incorporation of label into this ion was unaffected by the *acn1* mutation, reaching ~10% enrichment, as in the wild-type plants, whereas it was almost completely blocked by the *acs* mutation (Fig. 5B; Supplemental Dataset S2). This is a finding consistent with prior radioisotope studies that identified ACS as the acetate-activating enzyme in plastids (Kuhn et al., 1981).

Similar studies evaluated the flux of label from acetate through the cytosolic acetyl-CoA pool, which was tracked by analyzing the McLafferty fragment ion generated from the methyl ester of docosanoic acid (22:0). This fatty acid is considered to be generated by an endoplasmic reticulum-localized fatty acid elongase

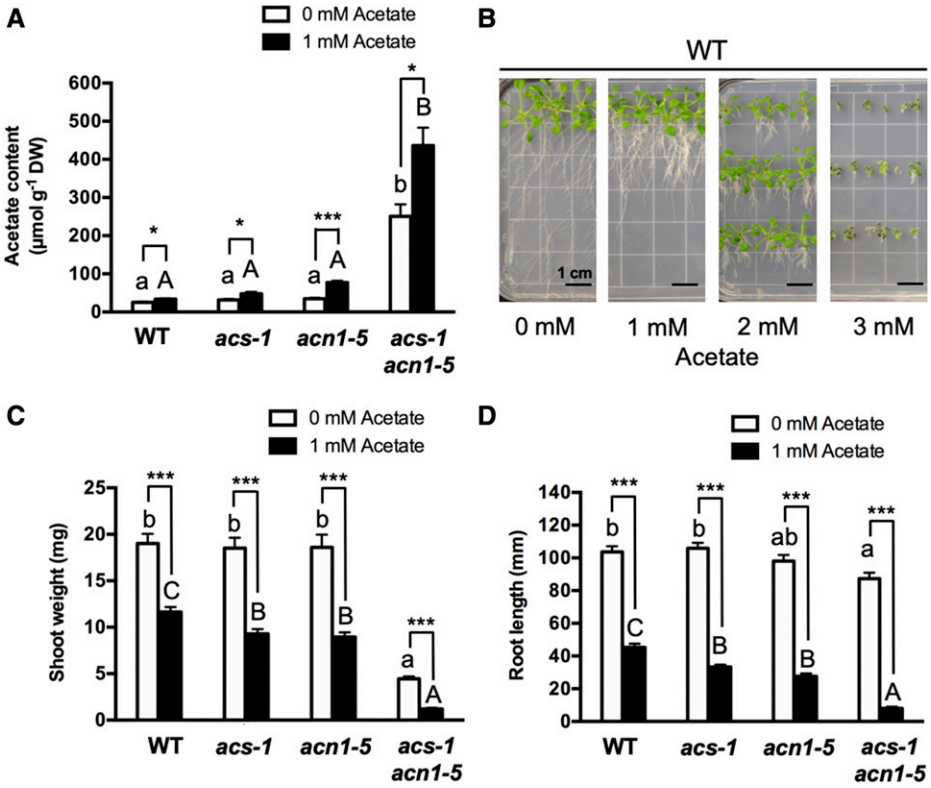

Figure 4. Effect of acetate on the growth of seedlings and on endogenous acetate levels. A, Acetate content in wild-type (WT) and mutant seedlings grown on media with or without 1 mM acetate. Values are means ± SE ($n > 3$). B, Wild-type Arabidopsis seedlings grown for 16 d on media supplemented with the indicated concentrations of acetate. C, Shoot weight of wild-type and mutant seedlings grown for 16 d on media with or without 1 mM acetate. Values are means ± SE ($n > 14$). D, Root length of the wild-type and mutant seedlings grown for 16 d on media with or without 1 mM acetate; values are means ± SE ($n > 14$). In A, C, and D, different letters above the data bars denote statistically significant differences among genotypes treated without acetate (lowercase letters) and among those treated with 1 mM acetate (uppercase letters) at $P < 0.05$ (calculated using one-way ANOVA followed by Tukey's test for multiple pairwise comparisons). Asterisks indicate statistically significant differences between plants treated with and without 1 mM acetate (*$P < 0.05$, ***$P < 0.001$; evaluated with Student's *t* test).

(Li-Beisson et al., 2010), which utilizes a preexisting acyl-CoA and elongates it with malonyl-CoA, generated from the cytosolic acetyl-CoA pool (Fig. 5A; Fatland et al., 2005). Figure 5B shows that label from acetate was incorporated more rapidly and more comprehensively into the cytosolic acetyl-CoA pool than the plastidic acetyl-CoA pool, and whereas the *acn1* mutation did not affect this incorporation, the *acs* mutation reduced the rate of incorporation by 50%. These data indicate that ACN1 does not contribute to the labeling of the cytosolic acetyl-CoA pool, but flux to this pool is partially attributable to ACS.

Analogous experiments tested whether plastidic ACS and peroxisomal ACN1 are involved in activating acetate generated from glycolytic intermediates. Similar to the acetate-labeling experiments, we evaluated whether the *acs* or *acn1* mutations affect the rates at which label is incorporated from [U-$^{13}C_6$]Glc into the McLafferty fragment ions generated from the fatty acids 16:0 and 22:0. Unlike the acetate labeling patterns, these experiments demonstrated that there is no difference in these rates among the three genotypes tested (Supplemental Fig. S3; Supplemental Dataset S3), indicating that neither ACS nor ACN1 is involved in generating the in vivo pool of plastidic and cytosolic acetyl-CoA pools from glycolytic intermediates. This is consistent with prior studies that established the in vivo physiological sources of these two acetyl-CoA pools, a plastid-localized pyruvate dehydrogenase complex (Bao et al., 2000; Lin et al., 2003) and a cytosol-localized ATP-citrate lyase (Fatland et al., 2005), respectively.

Kinetics of ^{13}C Labeling of Organic Acids and Amino Acids

The above [U-$^{13}C_2$]acetate- and [U-$^{13}C_6$]Glc-labeled seedlings were analyzed in parallel to evaluate the kinetics of label-incorporation into 19 amino acids and four organic acids. Compared to the wild type, the *acs* and *acn1* mutations did not affect any of the labeling patterns of amino acids and organic acids from [U-^{13}C]-Glc (Supplemental Figs. S4–S6; Supplemental Datasets S4 and S5), indicating that the metabolism of acetyl-CoA

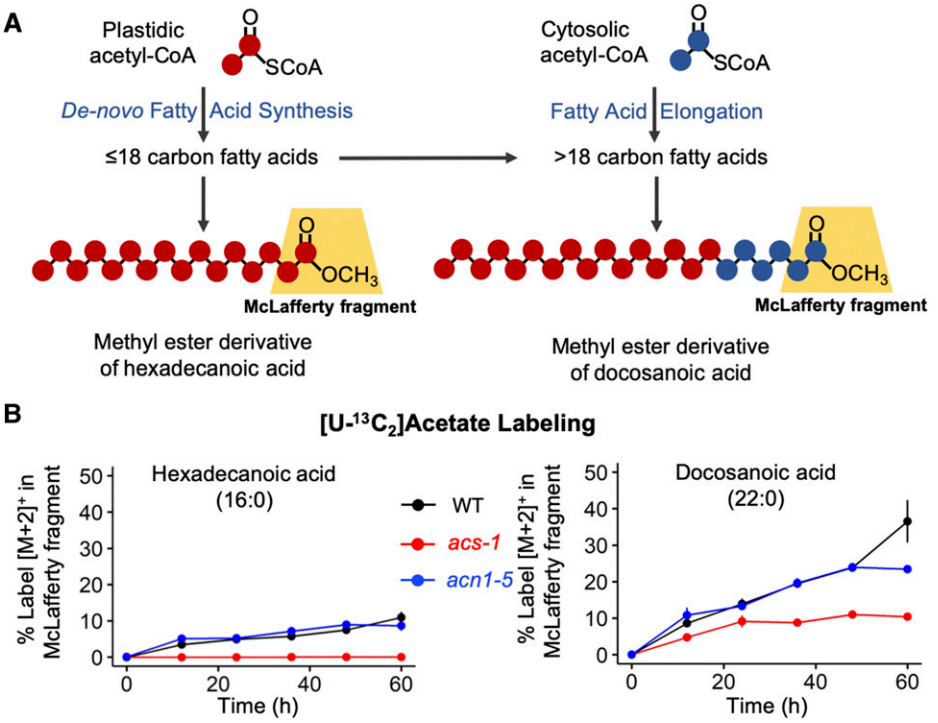

Figure 5. Kinetics of isotope incorporation from [U-$^{13}C_2$]acetate into the McLafferty ion of methyl ester derivatives of hexadecanoic acid (16:0) and docosanoic acid (22:0). A, Isotope incorporation into the 16:0- and 22:0-derived McLafferty ions reflects the metabolism through the plastidic and cytosolic acetyl-CoA pools, respectively. B, Time course of the incorporation of isotope by wild-type (WT), *acs-1*, and *acn1-5* seedlings incubated on media containing 1 mM [U-$^{13}C_2$]acetate. Fatty acids were extracted from whole seedlings and derivatized to fatty acid methyl esters and analyzed by GC-MS to determine the labeling of the $[M + 2]^+$ McLafferty ion. Values are means ± SE ($n = 4$). Statistically significant differences among the genotypes in the percent labeling of the $[M + 2]^+$ McLafferty ion at each time point are shown in Supplemental Dataset S2.

derived from the glycolytic pathway is not dependent on ACS and ACN1 functionality.

By contrast, both the *acs-1* and the *acn1-5* mutations inhibited the labeling kinetics of these amino acids and organic acids from [U-^{13}C]-acetate (Fig. 6; Supplemental Figs. S7 and D8; Supplemental Datasets S6 and S7). The most profound genetic modulator of these labeling patterns was the *acn1* mutation, which reduced the rate of labeling by 50% or more for many of these metabolites, including four organic acids (i.e. succinate, citrate, malate, and fumarate) and nine of the analyzed amino acids (i.e. Ser, Gly, Ala, Asp, Glu, Gln, GABA, Pro, and Orn). Previously, Allen et al. (2011) reported a similar reduction in labeling of Gln in the *acn1-2* mutant. We surmise from these observations that the ACN1-generated acetyl-CoA pool is a substrate for the glyoxylate cycle, labeling succinate, citrate, malate, and fumarate, and these organic acids can serve as substrates for amination or transamination reactions that generate amino acids such as Asp, Glu, Gln, GABA, Pro, and Orn (Owen et al., 2002; Hildebrandt et al., 2015). This supposition is consistent with the finding that the labeling patterns of the organic-acid precursors are similar to that of the amino acid products. In addition, the labeling patterns of the two photorespiratory intermediates (Ser and Gly) represent another mode for exporting the acetyl-unit from peroxisomes, in the form of acetyl-CoA (Reumann and Weber, 2006).

The single effect of the *acs* mutation was to reduce the rate of Leu labeling, which was not affected by the *acn1* mutation (Fig. 6). This Leu labeling was associated with the lower abundance of $[M + 2]^+$ ion (Supplemental Fig. S8), indicating that the acetyl group of the plastid-generated acetyl-CoA is directly incorporated into Leu, consistent with the fact that Leu is synthesized from plastidic pyruvate and acetyl-CoA (Binder, 2010).

Acetate Production via the Oxidation of Ethanol

Although the above genetic and labeling experiments defined the important roles of ACS and ACN1 for metabolizing acetate, the metabolic origin of this acetate is unclear. One potential source may be by oxidation of ethanol via the intermediate acetaldehyde, which is also associated with the PDH-bypass (Boubekeur et al., 1999). This potential was addressed by comparing the response of the wild-type and *acs-1* and *acn1-5* mutant seedlings grown in the presence of ethanol. The growth of wild-type and *acn1-5* mutant seedlings was unaffected by exposure to 20 mM ethanol, and the concentration of endogenous acetate was unaffected by this treatment. However, the response of the *acs-1* mutant was dramatically different. These seedlings showed significant growth phenotypic defects (Fig. 7A), and this was coupled with a 7-fold increase in endogenous acetate levels (Fig. 7B); both of these effects mirror the morphological and biochemical phenotypes presented by the *acs-1 acn1-5* double mutant (Figs. 1 and 4A). The coupling of growth aberrations with increased endogenous acetate levels was illustrated by titrating the ethanol exposure of the *acs-1* mutant seedlings. The data presented in Supplemental Figure S9 shows the direct correlation between the exposure to increasing ethanol concentration and a growth penalty, as well

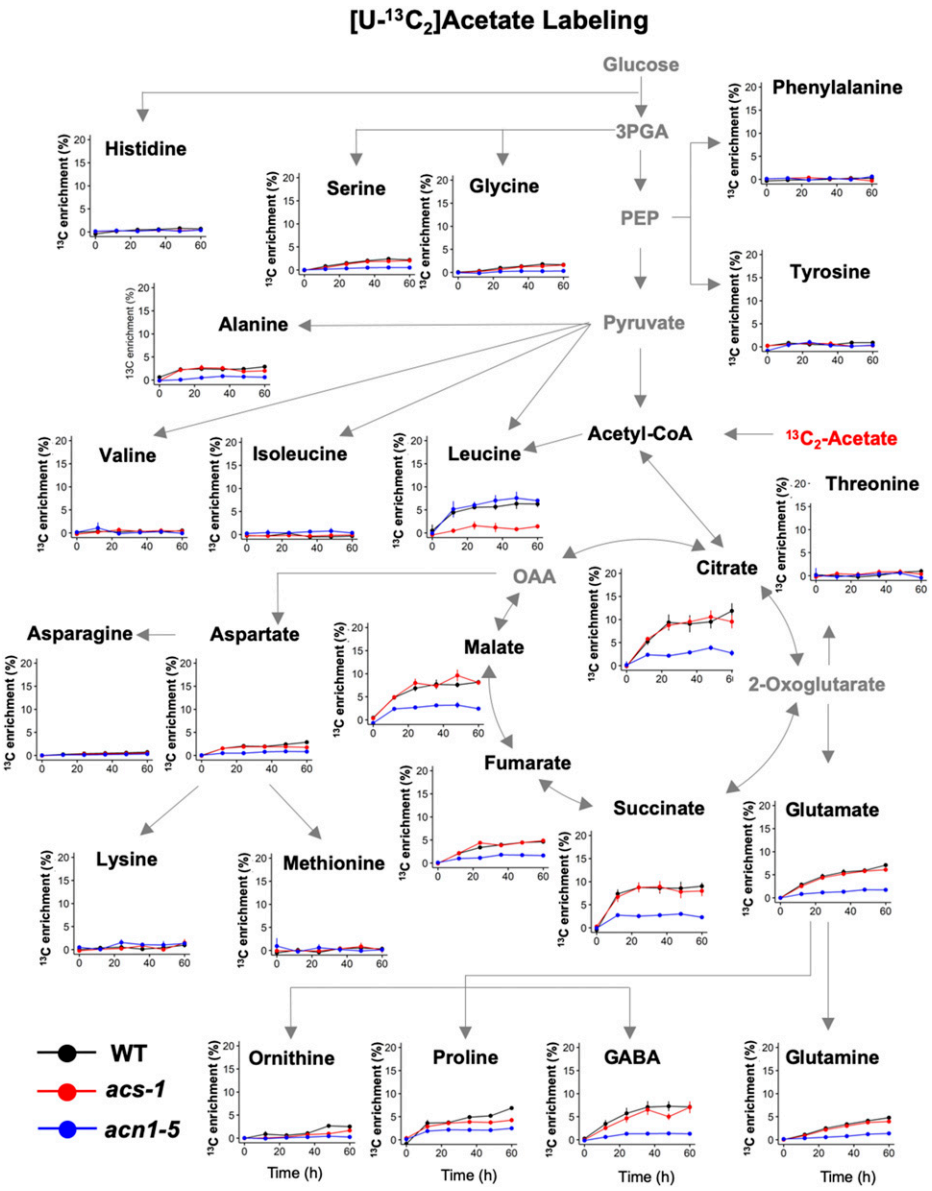

Figure 6. Pathway view of [U-$^{13}C_2$]acetate labeling kinetics of amino acids and organic acids. Time course of isotope labeling of wild-type (WT), *acs-1*, and *acn1-5* seedlings incubated with 1 mM [U-$^{13}C_2$]acetate. Polar metabolites were extracted from whole seedlings. Tert-butyldimethylsilyl derivatives of amino acids and organic acids were analyzed by GC-MS to determine mass isotopomer distributions. Mean ^{13}C enrichment was calculated as described in "Materials and Methods". Values are means ± SE (n = 4). Statistically significant differences among the genotypes in the percent ^{13}C enrichment of each metabolite at each time point are shown in Supplemental Dataset S6. Time courses of mass isotopomer distribution of these ^{13}C-labeled organic acids and amino acids are shown in Supplemental Figures S7 and S8, respectively.

as increasing endogenous acetate concentration. These data therefore indicate the predominant contribution of ACS in the removal of excess acetate produced from the oxidation of ethanol.

Further evidence that ethanol is a metabolic precursor of acetate was gained by using mutants in other enzymes required in this oxidation pathway, namely alcohol dehydrogenase (ADH), which generates acetaldehyde from ethanol, and aldehyde dehydrogenase (ALDH), which converts acetaldehyde to acetate. Specifically, we genetically combined the *acs* mutation with either *adh* or *aldh* mutations to generate double mutant stocks. This experiment was complicated by the fact that whereas ADH is encoded by a single gene (At1g77120), the Arabidopsis genome encodes potentially 14 ALDH isozymes (Stiti et al., 2011; Song et al., 2016). We specifically focused on the mitochondrial ALDH2B4 isozyme, which appears to be the major contributor to this pathway (Wei et al., 2009). Figure 7A shows that in plants carrying the combination of *acs* and *aldh2b4* mutations, the hyperaccumulation of acetate was blocked when these seedlings were challenged with exogenous ethanol. These results therefore establish the importance of ALDH2B4 in forming acetate from ethanol-derived acetaldehyde. However, the finding that the *acs-1 adh-1* double mutant only suppresses acetate hyperaccumulation from ethanol by ~30% (Fig. 7B) suggests that there is an alternative source of acetaldehyde.

Additional experiments were thus conducted to test whether this alternative source of acetaldehyde is via the nonoxidative decarboxylation of pyruvate, catalyzed by pyruvate decarboxylase (PDC), i.e. the PDH bypass (Boubekeur et al., 1999). Among the four genes encoding PDC in Arabidopsis, PDC1 and PDC2 are associated with hypoxic tolerance that generates

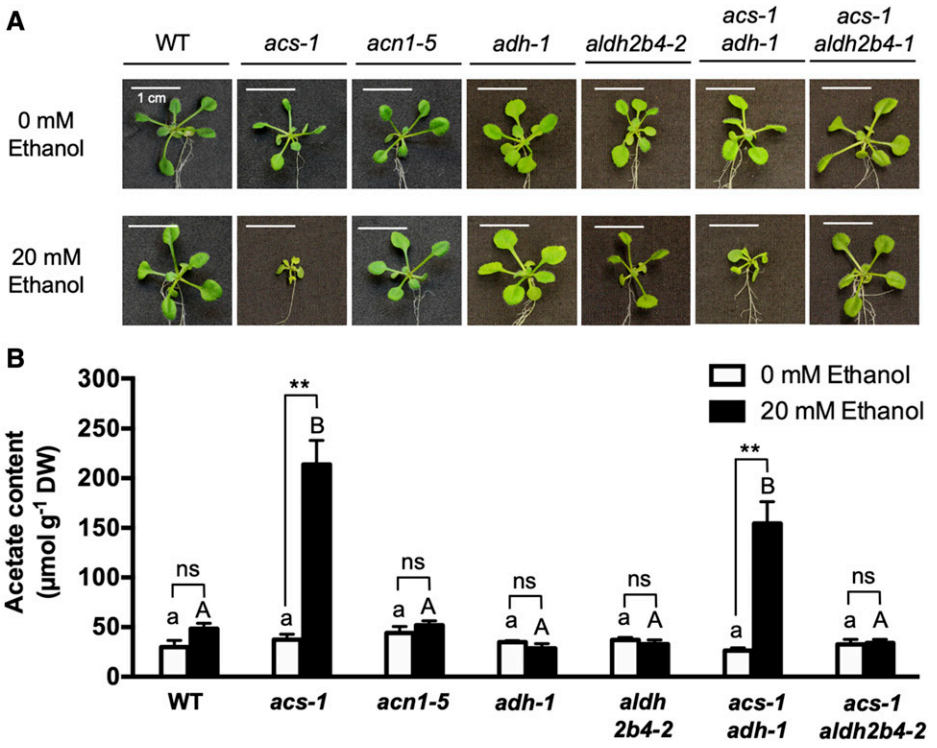

Figure 7. Effect of ethanol on the growth of seedlings and on endogenous acetate levels. A, Morphological phenotype of 16-d-old wild-type (WT) and mutant seedlings grown on media without ethanol or supplemented with 20 mM ethanol. B, Acetate content in wild-type and mutant seedlings grown with or without 20 mM ethanol. Values are means ± SE (n = 3–5). Different letters above the data bars denote statistically significant differences among the genotypes not treated with ethanol (lowercase letters) and those treated with 20 mM ethanol (uppercase letters); $P < 0.05$ (calculated by one-way ANOVA followed by Tukey's test for multiple pairwise comparisons). Asterisks indicate statistically significant differences between untreated plants and plants treated with 20 mM ethanol (**$P < 0.01$; ns, not significant; evaluated by Student's t test).

ethanol (Ismond et al., 2003; Mithran et al., 2014). Hence, we evaluated whether the incorporation of label into acetate from [U-$^{13}C_6$]Glc is affected by mutations in these PDC genes (Fig. 8A). With wild-type seedlings, the proportion of labeled acetate from [U-$^{13}C_6$]Glc was doubled when the seedlings were exposed to hypoxia (Fig. 8B). The involvement of PDC and ALDH in this conversion is indicated by the fact that the *pdc* mutation (specifically *pdc1*) and the *aldh* mutation (specifically *aldh2b4*) reduced this conversion by ~50% and ~80%, respectively, whereas the *pdc2* mutation did not have such an inhibitory effect (Fig. 8B). Further evidence supporting the involvement of PDC1 and ALDH2B4 in this conversion of Glc to acetate in hypoxia was obtained by the similarity in labeling patterns obtained with the *acs-1 aldh2b4-2* double mutant and the *acs-1 pdc1-1 pdc2-1* triple mutant (Fig. 8B).

DISCUSSION

Acetate Activation to Acetyl-CoA

The high-energy thioester bond that covalently links acetate and CoA to form acetyl-CoA has attributes that facilitate the role it plays as a key intermediate in metabolism, juxtaposed between anabolic and catabolic processes and linking central metabolism with specialized metabolism (Pietrocola et al., 2015). Indeed, it has been hypothesized that acetyl-CoA may have preceded the role of ATP as the common energy carrier in a so-called "thioester world" (de Duve, 1995).

Because of the cellular and subcellular compartmentalization that occurs in multicellular organisms, and because CoA-esters are membrane-impermeable molecules, the generation and utilization of acetyl-CoA is generally distributed in separate subcellular compartments to meet the dynamic physiological demands of the cell in response to different developmental and environmental cues. This is particularly apparent in plants, where multiple metabolic processes regulate the flux through acetyl-CoA pools in at least four subcellular compartments (Oliver et al., 2009). Although considerable research has been devoted to identifying the acetyl-CoA generation mechanisms in plastids (Huang and Stumpf, 1970; Ke et al., 2000; Schwender and Ohlrogge, 2002; Lin and Oliver, 2008), mitochondria (Thompson et al., 1977; Yu et al., 2012), peroxisomes (Hooks et al., 2004; Turner et al., 2005; Graham, 2008), and the cytosol (Fatland et al., 2002, 2005), the presence of redundant acetyl-CoA-generating enzymes and the difficulty of analyzing compartmentalized metabolism have posed a challenge of understanding the spatially and temporally regulated acetyl-CoA metabolism in separate subcellular compartments. In this study, we generated multimutant plant stocks and applied metabolomic profiling and stable isotope labeling strategies to characterize two distinctly localized acetate-activating systems (ACS and ACN1) and addressed their importance in the physiology and metabolism associated with growth and development.

The initial demonstration in the 1950s that isotopically labeled acetate can be incorporated into fatty acids (Newcomb and Stumpf, 1953) suggested that

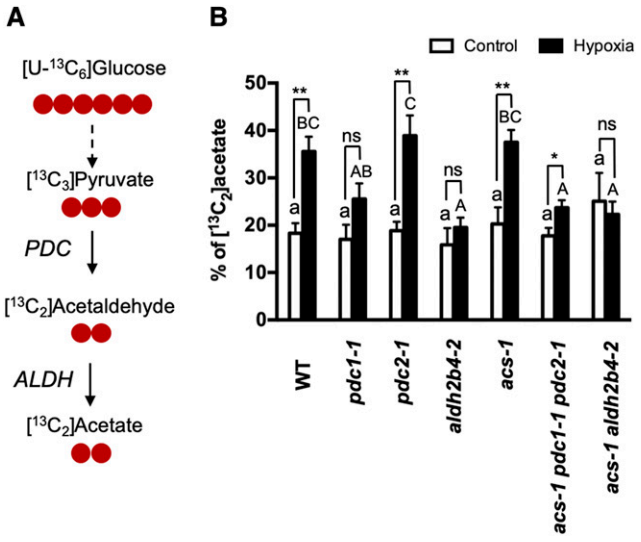

Figure 8. Effect of hypoxia on the incorporation of label from [U-$^{13}C_6$]Glc into acetate. A, Schematic representation of the metabolic process for the ^{13}C incorporation into acetate from [U-$^{13}C_6$]Glc. [U-$^{13}C_6$]Glc will generate [$^{13}C_3$]pyruvate through glycolysis. B, Wild-type (WT) and mutant Arabidopsis seedlings were cultured for 24 h in media supplemented with 10 mM [U-$^{13}C_6$]Glc in the presence or absence of hypoxia treatment. The ^{13}C enrichment of cellular acetate was quantitated with GC-MS. Values are means ± SE (n = 3–6). Different letters above the data bars denote statistically significant differences among the genotypes under control (lowercase letters) or hypoxia conditions (uppercase letters); $P < 0.05$ (calculated by one-way ANOVA followed by Tukey's test for multiple pairwise comparisons). Asterisks indicate statistically significant differences between the plants under control and hypoxia treatment (*$P < 0.05$, **$P < 0.01$; ns, not significant; evaluated by Student's t test).

AMP-forming ACS played a role in generating acetyl-CoA in plant cells. However, the in planta physiological role of this mechanism for generating this fatty acid precursor is unclear, because both genetic (Lin et al., 2003) and isotope labeling experiments (Bao et al., 2000) have established that the plastidic acetyl-CoA is predominantly generated from pyruvate, a reaction catalyzed by ptPDHC (Williams and Randall, 1979). More recently, ACN1 has been characterized as a peroxisomal enzyme that catalyzes the same AMP-forming activation of acetate, forming acetyl-CoA (Hooks et al., 2004; Turner et al., 2005). Allen et al. (2011) proposed that ACN1 prevents the loss of free acetate from peroxisomes during lipid mobilization. This is certainly possible, and if one assumes that this acetate is generated from the hydrolysis of acetyl-CoA (the product of β-oxidation of fatty acids), which would constitute an energy-consuming futile cycle. These findings therefore have left a dilemma concerning the physiological role of these two distinctly localized, acetate-activating enzymes.

The existence of two isozymes of ACSs in different subcellular locations has been characterized in many eukaryotes, including fungi and mammals (Fujino et al., 2001; Lee et al., 2011; Schug et al., 2016). In the case of *Saccharomyces cerevisiae*, the mitochondrial and cytosolic ACS isozymes are needed for growth on acetate and Glc, respectively, providing cells greater metabolic flexibility to changing environmental stimuli (Van den Berg and Steensma, 1995).

Combined Action of ACS and ACN1 Is Required for Maintaining Acetate Homeostasis and Normal Plant Growth

Prior genetic characterizations established that plants carrying either *acs* or *acn1* mutations are viable, without any obvious abnormal growth phenotype (Turner et al., 2005; Lin and Oliver, 2008). In this study, we unequivocally demonstrate that the combined functionality of the plastidic ACS and peroxisomal ACN1 are required for normal plant growth and development. Thus, the genetic loss of either isozyme can be compensated by the overlapping function(s) of the other enzyme, but genetically losing both enzymes is deleterious to normal growth. This parallels the findings in yeast, where the simultaneous disruption of both mitochondrial and cytosolic ACS isozymes is lethal (Van den Berg and Steensma, 1995), and this lethality may be associated with the inability to metabolize acetate, as overexpression of *ACS* in wild-type strains increases yeast tolerance to exogenous acetic acid (Ding et al., 2015).

The metabolic alterations that were displayed by the *acs-1 acn1-5* double mutant include the drastic reduction in the levels of many intermediates of central metabolism (i.e. amino acids, organic acids, sugars, and lipids) and the hyperaccumulation of acetate. These metabolic alternations were not observed in either the *acs-1* or *acn1-5* single mutants. Because neither of these mutations affects the normal acetyl-CoA-generating systems in plastids, via PDHC (Lin et al., 2003), or peroxisomes, via the β-oxidation pathway (Graham, 2008), the simultaneous absence of these two acetate-activating enzymes is unlikely to cause these growth and metabolic alterations due to lack of acetyl-CoA generation, but rather due to build-up of the substrate acetate. Indeed, the elevated accumulation of acetate in the *acs-1 acn1-5* double mutant is clear indication that, in combination, ACS and ACN1 are required to maintain acetate homeostasis and avoid the build-up of high levels of this carboxylate. The fact that high levels of exogenous acetate provided to wild-type plants causes a growth phenotype similar to that of the *acs-1 acn1-5* double mutant further supports this supposition that the build-up of acetate levels is causative of the growth defect. Consistent with this explanation are observations that the sensitivity to exogenous acetate is enhanced in both the *acs-1* and *acn1-5* single mutants, and even more enhanced in the double mutant, compared to the wild type.

Apparent inhibition of growth by acetate has previously been reported in seedlings (Turner et al., 2005) and cultured embryos (Pollard et al., 2015), and it is not an attribute unique to plants. High concentrations of

acetate inhibit growth of *Escherichia coli* (Luli and Strohl, 1990), *Saccharomyces cerevisiae* (Pampulha and Loureiro-Dias, 1989), and *Chlamydomonas reinhardtii* (Chen and Johns, 1994). Several mechanisms have been inferred from experiments with these microbial systems, including cellular acidification (Luli and Strohl, 1990; Jarboe et al., 2013), the induction of reactive oxygen species (Giannattasio et al., 2013), the inhibition of amino acid biosynthesis (Roe et al., 2002), and the reduction in intracellular ATP levels (Ding et al., 2013). In the *acs-1 acn1-5* double mutant, a rise in acetate level to ~20 mM on a plant-water basis would likely cause the cytoplasmic pH to fall by ~1 pH unit, assuming a buffering capacity of 15–30 mM per pH unit (Oja et al., 1999). Cytoplasmic acidification would activate pyruvate decarboxylase (Joshi et al., 2019), which enhances the formation of acetaldehyde that could potentially lead to induced acetate production.

The fact that acetate levels are elevated in both the *acs-1* and *acn1-5* single mutants, and are elevated to even more extreme levels in the *acs-1 acn1-5* double mutants, suggests that acetate can move across plastidic and peroxisomal membranes and be metabolized by the available acetate-activating enzyme in the alternate organelle in each single mutant. The interpretation of the results presented in this study has been guided by the findings that both the undissociated (i.e. acetic acid) and anionic forms of acetate can move across chloroplast membranes (Jacobson and Stumpf, 1972), but the acetate anion would dominate at physiological pH and may require active transporters to facilitate the transportation process. Monocarboxylate transporters that can facilitate the translocation of acetate have been commonly found in bacteria, yeast, and mammals (Paiva et al., 2004; Moschen et al., 2012; Sun et al., 2018), and the Arabidopsis ABC transporter *COMATOSE* (*CTS*) has been invoked in the transport of acetate into peroxisomes (Hooks et al., 2007).

Metabolic Origin of Acetate in Plants

When the *acs-1 acn1-5* double mutant seedlings are grown in the absence of exogenous acetate, the endogenous acetate level is increased 10-fold compared to that in the wild-type seedlings, which implies that acetate generation is a process that normally occurs during growth and development. This study provides evidence that one potential and possibly major mechanism for acetate production is through the oxidation of acetaldehyde, catalyzed by ALDH2B4, and additional ALDH isozymes could also contribute to this flux. Furthermore, there are two potential metabolic sources of acetaldehyde, ethanol oxidation catalyzed by alcohol dehydrogenase (Bicsak et al., 1982) or nonoxidative decarboxylation of pyruvate catalyzed by pyruvate decarboxylase (Ismond et al., 2003).

Evidence for the former mechanism is the accumulation of acetate in the *acs-1* mutant fed with ethanol, indicating the role of ACS in metabolizing ethanol-derived acetate. Although it is unclear why ACN1 is less efficient at detoxifying ethanol-derived acetate, exposure to increased concentrations of ethanol leads to toxic accumulation of acetate in the *acs-1* mutant. In contrast to the *acs-1* mutant, lowering of acetate levels in the ethanol-fed *acs-1 aldh2b4-2* double mutant establishes the key role of ALDH2B4 in converting ethanol-derived acetaldehyde to acetate. The involvement of ACS and ALDH in metabolizing ethanol to fatty acids via acetate has been implicated from prior observations of the incorporation of label from ^{14}C-ethanol into fatty acids (Cossins and Beevers, 1963; Mellema et al., 2002), and has been further substantiated by the observation that this rate of isotope labeling is reduced in the *acs-1* and *aldh2b4-2* mutants (Lin and Oliver, 2008; Wei et al., 2009).

Evidence for the second mechanism of acetaldehyde generation from pyruvate is supported by our ^{13}C-Glc labeling experiments highlighting the key roles of PDC1 and ALDH2B4 in this conversion, particularly during hypoxia. Prior observations detected a burst of acetaldehyde accumulation when plants are reintroduced to oxygen after a hypoxia treatment (Kreuzwieser et al., 1999; Boamfa et al., 2003; Copolovici and Niinemets, 2010). Thus, the ability of plants to convert acetaldehyde to acetate may be related to posthypoxic recovery (Nakazono et al., 2000; Tsuji et al., 2003). The labeling of acetate from [U-$^{13}C_6$]Glc in ambient conditions suggests that acetate formation via the PDH bypass occurs during normal aerobic conditions. The operation of the PDH bypass in such ambient conditions has been inferred in pollen (Tadege et al., 1999) and seedlings (Wei et al., 2009), and could occur in developing seeds with low internal oxygen concentrations (Rolletschek et al., 2005). In addition, the operation of the PDH bypass in aerobic tissues could be an adaptative response to episodic organellar thiamin diphosphate deficiency (Joshi et al., 2019).

Metabolic Fate of Acetate in Plant Cells

The metabolic fate of acetate catalyzed by either ACS- or ACN1-dependent activation to acetyl-CoA was delineated by tracing the dynamic incorporation of ^{13}C-labeled acetate into various downstream metabolites, as affected by mutations in each enzyme-coding gene. The acetyl-CoA pool generated by ACS can support the de novo synthesis of fatty acids and Leu, confirming prior characterizations of plastidic acetyl-CoA metabolism (Kuhn et al., 1981; Binder, 2010). On the other hand, the ACN1-generated acetyl-CoA pool provides the carbon backbones for synthesis of many organic acids (succinate, citrate, malate, and fumarate), as well as amino acids, many of which (Asp, Glu, Gln, GABA, Pro, Orn, Gly, and Ser) are derived from these organic acids. Because ACN1 is localized in peroxisomes, and these amino acids are not synthesized in this organelle, it is likely that the translocation of peroxisome-derived acetyl units is through the sequential action of peroxisomal citrate synthase, isocitrate

lyase, and malate synthase (Pracharoenwattana et al., 2005; Lingard et al., 2009), which generates anaplerotic substrates for the mitochondrial tricarboxylic acid cycle and thus leads to the labeling of amino acids from peroxisome-derived acetate.

Finally, our labeling experiments suggest the existence of an additional acetate-activating route in the cytosol that is independent of ACS and ACN1 functionality. This uncharacterized route is inferred to explain the incorporation of label from ^{13}C-acetate into cytosolic acetyl-CoA-derived fatty acids in both the *acs-1* and *acn1-5* single mutants. The near-identical labeling pattern of cytosolic acetyl-CoA-generated downstream metabolic products between the wild type and *acn1-5* mutants rules out the possibility that cytosolic acetyl-CoA is labeled from ^{13}C-acetate via peroxisomally generated citrate (Fatland et al., 2005), which can be labeled from the ACN1-generated acetyl-CoA pool. Thus, one potential source of a cytosolic acetyl-CoA-generating mechanism could be provided by the other 61 members in the acyl-activating enzyme superfamily, many of which display broad substrate ranges, in activating different carboxylic acids (Shockey and Browse, 2011). Indeed, Turner et al. (2005) reported acetyl-CoA synthetase enzymatic activity in extracts devoid of organelles, but one cannot discount the possibility that this was due to organelle disruption during the physical fractionation of the plant tissue extracts. Such an uncharacterized potentially cytosolic acetate-activating route could make use of the CTS transporter that utilizes the energy from ATP hydrolysis to translocate acyl-CoAs into peroxisomes (Hooks et al., 2007; Nyathi et al., 2010).

In summary, this study has revealed the important role of acetate metabolism in plants by genetically and metabolically characterizing two distinctly located acetate-activating enzymes (i.e. plastidic ACS and peroxisomal ACN1). Combined loss of the two enzymes leads to a dramatic increase in free acetate levels and decreases in the levels of many acetyl-CoA-derived downstream products of metabolism. These two redundant acetate-activating enzymes are thus required to prevent plants from accumulating deleterious levels of acetate, which can be mimicked by feeding either acetate or ethanol to wild-type plants. The results presented in this study provide further insights on interrelationships among different acetyl-CoA metabolic processes that are distributed among different subcellular compartments. Evidence presented herein integrates dynamic data (i.e. metabolic fluxes) with steady-state data (i.e. metabolite concentrations), which are consistent with prior studies indicating that maintaining acetate levels is critical to morphological stability (Pampulha and Loureiro-Dias, 1989; Luli and Strohl, 1990; Chen and Johns, 1994; Turner et al., 2005; Pollard et al., 2015). We suggest, therefore, that the evolutionary pressure to maintain acetate-activating enzymes (at least ACS and ACN1) is for sustaining acetate homeostasis, and to recover carbon that would otherwise be "lost" to metabolism as products of the PDH bypass and/or recovery from hypoxia stress conditions. Understanding the apparent toxic effect of disrupting this acetate homeostasis will require additional studies to directly assess the effects of altered in vivo pH due to acetate hyperaccumulation and altered compartment-specific acetyl-CoA metabolism caused by the inability to directly generate acetyl-CoA from acetate, and to distinguish between these effects.

MATERIALS AND METHODS

Plant Materials and Growth Conditions

Seed stocks of wild-type Arabidopsis (*Arabidopsis thaliana*, ecotype Col-0) and T-DNA insertional mutant lines were obtained from the ABRC (http://abrc.osu.edu/). The single knockout line *acs-1* (SALK_015522) has been described earlier (Lin and Oliver, 2008), and alleles *acs-2* (SALK_131620), *acn1-4* (SALK_009373C), and *acn1-5* (CS903402) are described herein. The two *acn1* mutant alleles used in this study are different from those previously characterized (i.e. *acn1-1*, *acn1-2*, and *acn1-3*; Hooks et al., 2004; Turner et al., 2005; Allen et al., 2011). In addition, the previously characterized *pdc1-1* (SALK_090204), *pdc2-1* (CS862662), *adh-1* (SALK_052699), and *aldh2b4-2* (SALK_078568) mutants were used for the ethanol feeding and hypoxia treatment experiments (Mithran et al., 2014; Song et al., 2016; Wei et al., 2009). All mutant alleles are in the Col-0 background.

Seeds were surface sterilized and scattered on one-half strength Murashige and Skoog agar medium supplemented with a vitamin mixture (Sigma-Aldrich). In the acetate and ethanol feeding experiments, the agar medium was supplemented with different concentrations of sodium acetate and ethanol, respectively. All media were adjusted to pH 5.7 before sterilization. Seeds were imbibed and stratified for 48 h at 4°C in darkness, and plants were grown under continuous illumination (100 μmol photons m^{-2} s^{-1}) at 22°C and 60% relative humidity. For the hypoxia treatment experiment, 16-d-old seedlings grown on agar plates were transferred into one-half strength Murashige and Skoog liquid medium containing 10 mM [U-$^{13}C_6$]Glc. Hypoxia was induced by flushing the liquid medium with nitrogen for 24 h to remove dissolved oxygen. As controls, a parallel set of plants was kept in the same liquid medium but under aerobic conditions for the duration of the experiment.

PCR-Based Genotyping and RT-PCR Analysis

PCR-based genotyping was conducted with template plant genomic DNA extracted from rosette leaves of individual plants as described previously (Sussman et al., 2000) and adapted to 96-well plate format. PCR reactions were conducted with GoTaq Green Master Mix (Promega) with allele-specific primer pairs (Supplemental Table S4). The resulting PCR products were analyzed by agarose gel electrophoresis. The precise T-DNA insertion positions in each allele of the *ACS* and *ACN1* genes were identified as the 18th intron for *acs-1*, the 12th intron for *acs-2*, the third exon for *acn1-4*, and the second exon for *acn1-5* (Supplemental Fig. S1A).

RT-PCR analysis was conducted on RNA isolated from plants using TriZol (Invitrogen). Contaminating DNA was removed by using a TURBO DNA-free kit (Invitrogen). RNA concentration was determined spectroscopically using a NanoDrop ND1000 Spectrophotometer (Thermo Fisher Scientific). Complementary DNA (cDNA) synthesis was conducted with a cDNA EcoDry Kit (Clontech) using 2 μg of RNA as the precursor. The resulting cDNA was used as the template for semiquantitative RT-PCR, performed with gene-specific primer pairs (Supplemental Table S5) and the GoTaq Green Master Mix (Promega).

Meiotic Recombination to Generate Multimutant Stocks

Double mutants targeting the ACS and ACN1 genes were generated by crossing homozygous plants carrying each of the *acs* mutant alleles with homozygous mutant plants carrying each of the *acn1* alleles. The *acs acn1* homozygous double mutant lines (i.e. *acs-1 acn1-4*, *acs-1 acn1-5*, *acs-2 acn1-4*, and *acs-2 acn1-5* double mutants) were detected in the F2 selfed progeny of the four pairwise

combinations of crosses, and these stocks were confirmed by PCR genotyping. For each of the four double mutant lines, families of >500 F2 plants were individually screened for aberrant phenotypes. Segregation ratios were determined by PCR genotyping of 200 individual F3 plants generated from the self-pollination of stocks that carried sesqui-mutant combinations of alleles. A statistical χ^2 goodness-of-fit test was used to determine whether the observed segregation ratios differ from the expected Mendelian segregation ratios. Similar intermating strategies were used to generate the *acs-1 adh-1* and *acs-1 aldh2b4-2* double mutant, and the *acs-1 pdc1-1 pdc2-1* triple mutant stocks.

Plant Phenotyping

Images of emerging seedlings and freshly opened flowers were obtained with a stereomicroscope (Macrozoom). Mature plants were imaged with a Nikon digital camera. Root length and rosette diameter were determined by quantifying the images using ImageJ software (http://imagej.nih.gov/ij/). Time to floral transition is defined as the interval from germination to the day of flower bolting. All measurements were carried out on 16 biological replicates. The significance of differences between the mutant plants and the wild type were assessed by ANOVA, followed by Dunnett's test for multiple comparisons of means using the R package "lsmeans" (Lenth, 2016).

Metabolite Profile Analysis

Leaves and roots of 16-d-old Arabidopsis seedlings from the mutant lines and wild type were rapidly collected, flash-frozen in liquid nitrogen, and lyophilized. Metabolites were extracted from preweighed dry tissues using the methanol/chloroform/water extraction protocol, as described previously (McVey et al., 2018). Known concentrations of nor-Leu and nonadecanoic acid were spiked onto the tissue, and these were used as internal quantification standards for polar and nonpolar fractions, respectively. The extracts were separated into two phases, facilitated by centrifugation, and the upper methanol-water phase (polar fraction) was removed, dried, and derivatized with methoxyamine hydrochloride and N,O-Bis(trimethylsilyl)trifluoroacetamide (BSTFA) with 1% (w/v) trimethylchlorosilane. The trimethylsilyl-derivatized polar samples were analyzed by a gas chromatography (GC)-MS system (an Agilent 6890 GC equipped with an Agilent HP-5ms column and interfaced to an Agilent 5973 MS) as described previously (McVey et al., 2018). The bottom, chloroform phase (nonpolar fraction) was dried separately and derivatized using 1 N methanolic HCl as described by Lu et al. (2008). The recovered fatty acid methyl esters (FAMEs) were quantified using a GC coupled to a flame ionization detector system (an Agilent 6890 GC equipped with an Agilent DB-1ms column). The chemical identity of each FAME was confirmed by MS with an Agilent 5973 MS. All peak areas were normalized relative to the peak areas of the internal standards (nor-Leu and nonadecanoic acid) and per sample dry weight. The averages from at least four biological replicates were used to determine the fold changes between each mutant line and the wild type. Student's *t* test was performed to identify the metabolites that changed concentrations between each mutant line and the wild type. The resultant *P*-values were corrected using the method of Benjamini and Hochberg (1995) to control the false discovery rate at 0.05, using R.

Quantification of Acetate

Seedlings were harvested, quenched in liquid nitrogen, and lyophilized. Preweighed dry samples were homogenized for 1 min at 30 Hz, using a Mixer Mill 301 (Retsch) with five Zirconia beads (2.3 mm; Biospec.com). Following addition of the internal standard [U-$^{13}C_2$]sodium acetate (99 atom % [w/w] ^{13}C; Sigma-Aldrich) at a rate of 4 μg/mg dry tissue, the tissue was extracted with 200 μL of HPLC-grade water. After sonication for 15 min and centrifugation at 16,000*g* for 10 min, 50 μL of the supernatant was diluted with an equal amount of HPLC-grade isopropanol, and the mixture was adjusted to pH 2–3 by the addition of 4 N HCl. The extracts were analyzed using a GC-MS system (an Agilent 6890 GC coupled to an Agilent 5975C MS) equipped with a nitroterephthalic acid-modified polyethylene glycol column (HP-FFAP; 30 m, 0.25-mm internal diameter, 0.25-μm film thickness; Agilent Technologies). An aliquot of the sample extract (2 μL) was injected in splitless mode with a helium carrier gas flow set at 2 mL/min, and the injector and transfer line temperatures were set to 260°C. The oven temperature was initially held at 60°C for 1 min, then raised to 120°C at 7.5°C/min, ramped to 240°C at 30°C/min, and kept at this temperature for 2 min. The MS was operated in selective-ion mode (electron impact at 70 eV, ion source temperature at 240°C), monitoring ions at *m/z* values of 60–62. Peak areas of unlabeled acetate (*m/z* 60) and the ^{13}C-labeled internal standard (*m/z* 62) were processed using Agilent ChemStation software. The amount of plant endogenous acetate was calculated using the standard isotope dilution method (Rittenberg and Foster, 1940). The fractional abundance of $^{13}C_2$-labeled acetate in the hypoxia-treatment experiment was determined with [1-$^{13}C_1$]sodium acetate (99 atom % [w/w] ^{13}C, Sigma-Aldrich) as the internal standard. The amount of unlabeled acetate (*m/z* 60) and $^{13}C_2$-labeled acetate (*m/z* 62) were calculated based on the $^{13}C_1$-labeled internal standard (*m/z* 61) using the isotope dilution method.

^{13}C-Isotope Kinetic Labeling

A liquid culture seedling system was utilized to monitor the kinetics of the incorporation of stable isotope from a defined substrate to downstream metabolites. This system enabled the rapid switch of the substrate of interest from the ^{12}C-labeled substrate to the ^{13}C-labeled substrate (Yuan et al., 2008; Evans et al., 2018). Specifically, sterilized seeds were germinated in 125-mL sterile Erlenmeyer glass flasks containing 50 mL of one-half strength Murashige and Skoog liquid medium at pH 5.7 (adjusted as needed with KOH) supplemented with either 1 mM sodium ^{12}C-acetate or 10 mM ^{12}C-Glc. These flasks were arranged in a randomized complete block design on a platform shaker (120 rpm) under continuous illumination (100 μmol photons m^{-2} s^{-1}) at a temperature of 22°C. After a 15-d incubation period, seedlings were rapidly switched into flasks containing medium that was identical except that it included either 1 mM [U-$^{13}C_2$]sodium acetate or 10 mM [U-$^{13}C_6$]Glc. This medium switch was staggered so that after 60 h, seedlings in different flasks were exposed to the isotope labeled medium for 12, 24, 36, 48, or 60 h. The whole seedlings were then quickly collected by filtration, washed three times with one-half strength Murashige and Skoog medium, quenched by flash-freezing in liquid nitrogen, lyophilized, and stored at −80°C until analysis.

GC-MS Analysis of Isotopic Labeling Patterns

Extraction of intracellular metabolites and analysis by GC-MS was performed as described above ("Metabolite Profile Analysis") using an Agilent 6890 GC equipped with an Agilent HP-5ms column and coupled to an Agilent 5973 MS. All measurements were carried out on whole seedlings with four biological replicates. The fatty acids recovered in the nonpolar fraction were converted to FAMEs as described previously (Lu et al., 2008). The McLafferty fragment ions (*m/z* 74) from individual FAMEs contained the C1 and C2 of saturated fatty acids. The fractional labeling of these two terminal carbon atoms of each fatty acid was determined by analysis of the *m/z* 74–76 ion cluster (Schwender and Ohlrogge, 2002). Amino acids and organic acids recovered in the polar fraction were derivatized in anhydrous pyridine with N-(*tert*-butyldimethylsilyl)-N-methyltrifluoroacetamide and 1% (w/v) *tert*-butyldimethylchlorosilane as described by Young et al. (2014). The resulting *tert*-butyldimethylsilyl derivatives produce characteristic mass-spectrometric fragment ions, as described earlier (Antoniewicz et al., 2007; Young et al., 2014). Supplemental Table S6 identifies these characteristic fragment ions that were used for the isotopomer analysis and the number of carbon atoms that could be labeled in the evaluated amino acids and organic acids. Extracted ion chromatograms for each isotopomer were integrated using DExSI 1.11 (Dagley and McConville, 2018) to generate mass isotopomer distribution, which describes the fractional abundances of each mass isotopomer for a metabolite (Buescher et al., 2015). A metabolite with x carbon atoms can have x mass isotopomers with the *m/z* range from M to $M + x$; the sum of the fractional abundances from M to $M + x$ is 100%. The measured mass isotopomer distributions were corrected for natural isotope abundance using Fluxfix 0.1 (Trefely et al., 2016). The mean ^{13}C enrichment for each metabolite is the weighted sum of the fractional abundance of each mass isotopomer, as described earlier (Schwender and Ohlrogge, 2002; Szecowka et al., 2013).

Accession Numbers

Sequence data from this article can be found in the GenBank/EMBL data libraries under the following accession numbers: At5g36880 (ACS; gene identification [ID] 833655); At3g16910 (ACN1; gene ID 820946); At1g77120 (*ADH*; gene ID 844047); At3g48000 (*ALDH2B4*; gene ID 823955); At4g33070 (*PDC1*; gene ID 829444); and At5g54960 (*PDC2*; gene ID 835587).

Supplemental Materials

The following supplemental materials are available.

Supplemental Figure S1. Identification of *acs* and *acn1* mutant alleles.

Supplemental Figure S2. Development of progeny from *acs-1 acn1-5* sesqui-mutant seedlings.

Supplemental Figure S3. Kinetics of the isotope incorporation from [U-$^{13}C_6$]Glc into the McLafferty fragments of methyl ester derivatives of hexadecanoic acid (16:0) and docosanoic acid (22:0) by wild-type, *acs-1*, and *acn1-5* mutant seedlings incubated on media containing 10 mM [U-$^{13}C_6$]Glc.

Supplemental Figure S4. Pathway view of [U-$^{13}C_6$]Glc labeling kinetics of amino acids and organic acids.

Supplemental Figure S5. Time course of mass isotopomer distribution of ^{13}C-labeled organic acids from [U-$^{13}C_6$]Glc.

Supplemental Figure S6. Time course of mass isotopomer distribution of ^{13}C-labeled amino acids from [U-$^{13}C_6$]Glc.

Supplemental Figure S7. Time course of mass isotopomer distribution of ^{13}C-labeled organic acids from [U-$^{13}C_2$]acetate.

Supplemental Figure S8. Time course of mass isotopomer distribution of ^{13}C-labeled of amino acids from [U-$^{13}C_2$]acetate.

Supplemental Figure S9. Effect of ethanol dose on growth of seedlings and endogenous acetate levels.

Supplemental Table S1. Growth characteristics of *acs* and *acn1* single mutants, and *acs-1 acn1-5* sesqui- and double mutants.

Supplemental Table S2. Phenotype segregation in the F2 generation from *acs acn1* heterozygous double mutant parents.

Supplemental Table S3. Segregation analysis of F3 progeny from two sesqui-mutant lines.

Supplemental Table S4. Sequences of the DNA primer pairs used in PCR analyses in this study.

Supplemental Table S5. Sequences of the DNA primer pairs used for RT-PCR analysis.

Supplemental Table S6. GC-MS fragments of tert-butyldimethylsilyl-derivatized amino acids and organic acids.

Supplemental Dataset S1. Metabolite profiling revealed differential metabolic changes of *acs-1* and *acn1-5* mutant seedlings.

Supplemental Dataset S2. Differences in ^{13}C enrichment of terminal acetyl groups of 16:0 and 22:0 fatty acids after labeling with [U-$^{13}C_2$]acetate.

Supplemental Dataset S3. Differences in ^{13}C enrichment of terminal acetyl groups of 16:0 and 22:0 fatty acids after labeling with [U-$^{13}C_6$]Glc.

Supplemental Dataset S4. Differences in average percent of ^{13}C enrichment of organic acids and amino acids after labeling with [U-$^{13}C_6$]Glc.

Supplemental Dataset S5. Differences in percent abundance of each isotopomer in organic acids and amino acids after labeling with [U-$^{13}C_6$]Glc.

Supplemental Dataset S6. Differences in average percent ^{13}C enrichment of organic acids and amino acids after labeling with [U-$^{13}C_2$]acetate.

Supplemental Dataset S7. Differences in percent abundance of each isotopomer in organic acids and amino acids after labeling with [U-$^{13}C_2$]acetate.

ACKNOWLEDGMENTS

The authors acknowledge the W. M. Keck Metabolomics Research Laboratory (Iowa State University) for guidance in the metabolic analyses; the Roy J. Carver High Resolution Microscopy Facility (Iowa State University) for providing access to the Macrozoom imaging system; and Rachel Garlock and Rahne McIntire (Iowa State University) for assisting with screening for plant mutants.

Received November 19, 2019; accepted December 12, 2019; published December 24, 2019.

LITERATURE CITED

Allen E, Moing A, Wattis JA, Larson T, Maucourt M, Graham IA, Rolin D, Hooks MA (2011) Evidence that ACN1 (acetate non-utilizing 1) prevents carbon leakage from peroxisomes during lipid mobilization in *Arabidopsis* seedlings. Biochem J **437:** 505–513

Antoniewicz MR, Kelleher JK, Stephanopoulos G (2007) Accurate assessment of amino acid mass isotopomer distributions for metabolic flux analysis. Anal Chem **79:** 7554–7559

Bao X, Focke M, Pollard M, Ohlrogge J (2000) Understanding in vivo carbon precursor supply for fatty acid synthesis in leaf tissue. Plant J **22:** 39–50

Benjamini Y, Hochberg Y (1995) Controlling the false discovery rate: A practical and powerful approach to multiple testing. J R Stat Soc Series B Stat Methodol **57:** 289–300

Bicsak TA, Kann LR, Reiter A, Chase T Jr. (1982) Tomato alcohol dehydrogenase: Purification and substrate specificity. Arch Biochem Biophys **216:** 605–615

Binder S (2010) Branched-chain amino acid metabolism in *Arabidopsis thaliana*. The Arabidopsis Book **8:** e0137. Available at: 10.1199/tab.0137

Boamfa EI, Ram PC, Jackson MB, Reuss J, Harren FJM (2003) Dynamic aspects of alcoholic fermentation of rice seedlings in response to anaerobiosis and to complete submergence: Relationship to submergence tolerance. Ann Bot **91:** 279–290

Boubekeur S, Bunoust O, Camougrand N, Castroviejo M, Rigoulet M, Guérin B (1999) A mitochondrial pyruvate dehydrogenase bypass in the yeast *Saccharomyces cerevisiae*. J Biol Chem **274:** 21044–21048

Boyes DC, Zayed AM, Ascenzi R, McCaskill AJ, Hoffman NE, Davis KR, Görlach J (2001) Growth stage-based phenotypic analysis of Arabidopsis: A model for high throughput functional genomics in plants. Plant Cell **13:** 1499–1510

Buescher JM, Antoniewicz MR, Boros LG, Burgess SC, Brunengraber H, Clish CB, DeBerardinis RJ, Feron O, Frezza C, Ghesquiere B, et al (2015) A roadmap for interpreting ^{13}C metabolite labeling patterns from cells. Curr Opin Biotechnol **34:** 189–201

Chen F, Johns MR (1994) Substrate inhibition of *Chlamydomonas reinhardtii* by acetate in heterotrophic culture. Process Biochem **29:** 245–252

Copolovici L, Niinemets U (2010) Flooding induced emissions of volatile signalling compounds in three tree species with differing waterlogging tolerance. Plant Cell Environ **33:** 1582–1594

Cossins EA, Beevers H (1963) Ethanol metabolism in plant tissues. Plant Physiol **38:** 375–380

Dagley MJ, McConville MJ (2018) DExSI: A new tool for the rapid quantitation of ^{13}C-labelled metabolites detected by GC-MS. Bioinformatics **34:** 1957–1958

de Duve C (1995) The beginnings of life on earth. Am Sci **83:** 428–437

Ding J, Bierma J, Smith MR, Poliner E, Wolfe C, Hadduck AN, Zara S, Jirikovic M, van Zee K, Penner MH, et al (2013) Acetic acid inhibits nutrient uptake in *Saccharomyces cerevisiae*: Auxotrophy confounds the use of yeast deletion libraries for strain improvement. Appl Microbiol Biotechnol **97:** 7405–7416

Ding J, Holzwarth G, Penner MH, Patton-Vogt J, Bakalinsky AT (2015) Overexpression of acetyl-CoA synthetase in *Saccharomyces cerevisiae* increases acetic acid tolerance. FEMS Microbiol Lett **362:** 1–7

Evans EM, Freund DM, Sondervan VM, Cohen JD, Hegeman AD (2018) Metabolic patterns in *Spirodela polyrhiza* revealed by ^{15}N stable isotope labeling of amino acids in photoautotrophic, heterotrophic, and mixotrophic growth conditions. Front Chem **6:** 191

Fatland BL, Ke J, Anderson MD, Mentzen WI, Cui LW, Allred CC, Johnston JL, Nikolau BJ, Wurtele ES (2002) Molecular characterization of a heteromeric ATP-citrate lyase that generates cytosolic acetyl-coenzyme A in Arabidopsis. Plant Physiol **130:** 740–756

Fatland BL, Nikolau BJ, Wurtele ES (2005) Reverse genetic characterization of cytosolic acetyl-CoA generation by ATP-citrate lyase in Arabidopsis. Plant Cell **17:** 182–203

Fujino T, Kondo J, Ishikawa M, Morikawa K, Yamamoto TT (2001) Acetyl-CoA synthetase 2, a mitochondrial matrix enzyme involved in the oxidation of acetate. J Biol Chem **276:** 11420–11426

Galdieri L, Zhang T, Rogerson D, Lleshi R, Vancura A (2014) Protein acetylation and acetyl coenzyme a metabolism in budding yeast. Eukaryot Cell **13:** 1472–1483

Giannattasio S, Guaragnella N, Zdralević M, Marra E (2013) Molecular mechanisms of *Saccharomyces cerevisiae* stress adaptation and programmed cell death in response to acetic acid. Front Microbiol **4:** 33

Graham IA (2008) Seed storage oil mobilization. Annu Rev Plant Biol **59:** 115–142

Hildebrandt TM, Nunes Nesi A, Araújo WL, Braun HP (2015) Amino acid catabolism in plants. Mol Plant **8:** 1563–1579

Hooks MA, Turner JE, Murphy EC, Graham IA (2004) Acetate non-utilizing mutants of Arabidopsis: Evidence that organic acids influence carbohydrate perception in germinating seedlings. Mol Genet Genomics **271:** 249–256

Hooks MA, Turner JE, Murphy EC, Johnston KA, Burr S, Jarosławski S (2007) The *Arabidopsis* ALDP protein homologue COMATOSE is instrumental in peroxisomal acetate metabolism. Biochem J **406:** 399–406

Huang KP, Stumpf PK (1970) Fat metabolism in higher plants. XLI. Properties of potato acetyl coenzyme A synthetase. Arch Biochem Biophys **140:** 158–173

Ismond KP, Dolferus R, de Pauw M, Dennis ES, Good AG (2003) Enhanced low oxygen survival in Arabidopsis through increased metabolic flux in the fermentative pathway. Plant Physiol **132:** 1292–1302

Jacobson BS, Stumpf PK (1972) Fat metabolism in higher plants. LV. Acetate uptake and accumulation by class I and II chloroplasts from *Spinacia oleracea*. Arch Biochem Biophys **153:** 656–663

Jarboe LR, Royce LA, Liu P (2013) Understanding biocatalyst inhibition by carboxylic acids. Front Microbiol **4:** 272

Joshi J, Folz JS, Gregory JF III, McCarty DR, Fiehn O, Hanson AD (2019) Rethinking the PDH bypass and GABA shunt as thiamin-deficiency workarounds. Plant Physiol **181:** 389–393

Ke J, Behal RH, Back SL, Nikolau BJ, Wurtele ES, Oliver DJ (2000) The role of pyruvate dehydrogenase and acetyl-coenzyme A synthetase in fatty acid synthesis in developing Arabidopsis seeds. Plant Physiol **123:** 497–508

Kreuzwieser J, Scheerer U, Rennenberg H (1999) Metabolic origin of acetaldehyde emitted by poplar (*Populus tremula* × *P. alba*) trees. J Exp Bot **50:** 757–765

Krivoruchko A, Zhang Y, Siewers V, Chen Y, Nielsen J (2015) Microbial acetyl-CoA metabolism and metabolic engineering. Metab Eng **28:** 28–42

Kuhn DN, Knauf M, Stumpf PK (1981) Subcellular localization of acetyl-CoA synthetase in leaf protoplasts of *Spinacia oleracea*. Arch Biochem Biophys **209:** 441–450

Lee S, Son H, Lee J, Min K, Choi GJ, Kim J-C, Lee Y-W (2011) Functional analyses of two acetyl coenzyme A synthetases in the ascomycete *Gibberella zeae*. Eukaryot Cell **10:** 1043–1052

Lenth RV (2016) Least-squares means: The R package lsmeans. J Stat Softw **69:** 1–33

Li-Beisson Y, Shorrosh B, Beisson F, Andersson MX, Arondel V, Bates PD, Baud S, Bird D, Debono A, Durrett TP, et al (2010) Acyl-lipid metabolism. The Arabidopsis Book **8:** e0133. Available at: 10.1199/tab.0133

Liedvogel B, Stumpf PK (1982) Origin of acetate in spinach leaf cell. Plant Physiol **69:** 897–903

Lin M, Behal R, Oliver DJ (2003) Disruption of *plE2*, the gene for the E2 subunit of the plastid pyruvate dehydrogenase complex, in *Arabidopsis* causes an early embryo lethal phenotype. Plant Mol Biol **52:** 865–872

Lin M, Oliver DJ (2008) The role of acetyl-coenzyme A synthetase in Arabidopsis. Plant Physiol **147:** 1822–1829

Lingard MJ, Monroe-Augustus M, Bartel B (2009) Peroxisome-associated matrix protein degradation in *Arabidopsis*. Proc Natl Acad Sci USA **106:** 4561–4566

Lu Y, Savage LJ, Ajjawi I, Imre KM, Yoder DW, Benning C, Dellapenna D, Ohlrogge JB, Osteryoung KW, Weber AP, et al (2008) New connections across pathways and cellular processes: Industrialized mutant screening reveals novel associations between diverse phenotypes in Arabidopsis. Plant Physiol **146:** 1482–1500

Luli GW, Strohl WR (1990) Comparison of growth, acetate production, and acetate inhibition of *Escherichia coli* strains in batch and fed-batch fermentations. Appl Environ Microbiol **56:** 1004–1011

McLafferty FW (1959) Mass spectrometric analysis. Molecular rearrangements. Anal Chem **31:** 82–87

McVey PA, Alexander LE, Fu X, Xie B, Galayda K-J, Nikolau BJ, Houk RS (2018) Light-dependent changes in the spatial localization of metabolites in *Solenostemon scutellarioides* (Coleus Henna) visualized by matrix-free atmospheric pressure electrospray laser desorption ionization mass spectrometry imaging. Front Plant Sci **9:** 1348

Mellema S, Eichenberger W, Rawyler A, Suter M, Tadege M, Kuhlemeier C (2002) The ethanolic fermentation pathway supports respiration and lipid biosynthesis in tobacco pollen. Plant J **30:** 329–336

Mithran M, Paparelli E, Novi G, Perata P, Loreti E (2014) Analysis of the role of the pyruvate decarboxylase gene family in *Arabidopsis thaliana* under low-oxygen conditions. Plant Biol (Stuttg) **16:** 28–34

Moschen I, Bröer A, Galić S, Lang F, Bröer S (2012) Significance of short chain fatty acid transport by members of the monocarboxylate transporter family (MCT). Neurochem Res **37:** 2562–2568

Nakazono M, Tsuji H, Li Y, Saisho D, Arimura S, Tsutsumi N, Hirai A (2000) Expression of a gene encoding mitochondrial aldehyde dehydrogenase in rice increases under submerged conditions. Plant Physiol **124:** 587–598

Nyathi Y, De Marcos Lousa C, van Roermund CW, Wanders RJ, Johnson B, Baldwin SA, Theodoulou FL, Baker A (2010) The *Arabidopsis* peroxisomal ABC transporter, Comatose, complements the *Saccharomyces cerevisiae pxa1 pxa2Δ* mutant for metabolism of long-chain fatty acids and exhibits fatty acyl-CoA-stimulated ATPase activity. J Biol Chem **285:** 29892–29902

Newcomb EH, Stumpf PK (1953) Fat metabolism in higher plants. I. Biogenesis of higher fatty acids by slices of peanut cotyledons in vitro. J Biol Chem **200:** 233–239

Oja V, Savchenko G, Jakob B, Heber U (1999) pH and buffer capacities of apoplastic and cytoplasmic cell compartments in leaves. Planta **209:** 239–249

Oliver DJ, Nikolau BJ, Wurtele ES (2009) Acetyl-CoA—Life at the metabolic nexus. Plant Sci **176:** 597–601

Owen OE, Kalhan SC, Hanson RW (2002) The key role of anaplerosis and cataplerosis for citric acid cycle function. J Biol Chem **277:** 30409–30412

Pampulha ME, Loureiro-Dias MC (1989) Combined effect of acetic acid, pH and ethanol on intracellular pH of fermenting yeast. Appl Microbiol Biotechnol **31:** 547–550

Paiva S, Devaux F, Barbosa S, Jacq C, Casal M (2004) Ady2p is essential for the acetate permease activity in the yeast *Saccharomyces cerevisiae*. Yeast **21:** 201–210

Pietrocola F, Galluzzi L, Bravo-San Pedro JM, Madeo F, Kroemer G (2015) Acetyl coenzyme A: A central metabolite and second messenger. Cell Metab **21:** 805–821

Pollard M, Delamarter D, Martin T, Shachar-Hill Y (2015) Lipid labeling from acetate or glycerol in cultured embryos of *Camelina sativa* seeds: A tale of two substrates. Phytochemistry **118:** 192–203

Pracharoenwattana I, Cornah JE, Smith SM (2005) Arabidopsis peroxisomal citrate synthase is required for fatty acid respiration and seed germination. Plant Cell **17:** 2037–2048

Reumann S, Weber APM (2006) Plant peroxisomes respire in the light: Some gaps of the photorespiratory C2 cycle have become filled—others remain. Biochim Biophys Acta **1763:** 1496–1510

Rittenberg D, Foster GL (1940) A new procedure for quantitative analysis by isotope dilution, with application to the determination of amino acids and fatty acids. J Biol Chem **133:** 737–744

Roe AJ, O'Byrne C, McLaggan D, Booth IR (2002) Inhibition of *Escherichia coli* growth by acetic acid: A problem with methionine biosynthesis and homocysteine toxicity. Microbiology **148:** 2215–2222

Rolletschek H, Koch K, Wobus U, Borisjuk L (2005) Positional cues for the starch/lipid balance in maize kernels and resource partitioning to the embryo. Plant J **42:** 69–83

Roughan PG, Holland R, Slack CR (1979) Acetate is the preferred substrate for long-chain fatty acid synthesis in isolated spinach chloroplasts. Biochem J **184:** 565–569

Schug ZT, Vande Voorde J, Gottlieb E (2016) The metabolic fate of acetate in cancer. Nat Rev Cancer **16:** 708–717

Schwender J, Ohlrogge JB (2002) Probing in vivo metabolism by stable isotope labeling of storage lipids and proteins in developing *Brassica napus* embryos. Plant Physiol **130:** 347–361

Shockey JM, Fulda MS, Browse J (2003) Arabidopsis contains a large superfamily of acyl-activating enzymes. Phylogenetic and biochemical analysis reveals a new class of acyl-coenzyme a synthetases. Plant Physiol **132:** 1065–1076

Shockey J, Browse J (2011) Genome-level and biochemical diversity of the acyl-activating enzyme superfamily in plants. Plant J **66:** 143–160

Sofeo N, Hart JH, Butler B, Oliver DJ, Yandeau-Nelson MD, Nikolau BJ (2019) Altering the substrate specificity of acetyl-CoA synthetase by rational mutagenesis of the carboxylate binding pocket. ACS Synth Biol **8:** 1325–1336

Song Y, Liu L, Wei Y, Li G, Yue X, An L (2016) Metabolite profiling of *adh1* mutant response to cold stress in *Arabidopsis*. Front Plant Sci **7:** 2072

Stiti N, Missihoun TD, Kotchoni SO, Kirch H-H, Bartels D (2011) Aldehyde dehydrogenases in *Arabidopsis thaliana*: Biochemical requirements, metabolic pathways, and functional analysis. Front Plant Sci **2:** 65

Sun P, Li J, Zhang X, Guan Z, Xiao Q, Zhao C, Song M, Zhou Y, Mou L, Ke M, et al (2018) Crystal structure of the bacterial acetate transporter SatP reveals that it forms a hexameric channel. J Biol Chem **293:** 19492–19500

Sussman MR, Amasino RM, Young JC, Krysan PJ, Austin-Phillips S (2000) The Arabidopsis knockout facility at the University of Wisconsin-Madison. Plant Physiol **124:** 1465–1467

Szecowka M, Heise R, Tohge T, Nunes-Nesi A, Vosloh D, Huege J, Feil R, Lunn J, Nikoloski Z, Stitt M, et al (2013) Metabolic fluxes in an illuminated *Arabidopsis* rosette. Plant Cell **25:** 694–714

Tadege M, Dupuis I, Kuhlemeier C (1999) Ethanolic fermentation: New functions for an old pathway. Trends Plant Sci **4:** 320–325

Thompson P, Reid EE, Lyttle CR, Dennis DT (1977) Pyruvate dehydrogenase complex from higher plant mitochondria and proplastids: Regulation. Plant Physiol **59:** 854–858

Trefely S, Ashwell P, Snyder NW (2016) FluxFix: Automatic isotopologue normalization for metabolic tracer analysis. BMC Bioinformatics **17:** 485

Tsuji H, Meguro N, Suzuki Y, Tsutsumi N, Hirai A, Nakazono M (2003) Induction of mitochondrial aldehyde dehydrogenase by submergence facilitates oxidation of acetaldehyde during re-aeration in rice. FEBS Lett **546:** 369–373

Turner JE, Greville K, Murphy EC, Hooks MA (2005) Characterization of *Arabidopsis* fluoroacetate-resistant mutants reveals the principal mechanism of acetate activation for entry into the glyoxylate cycle. J Biol Chem **280:** 2780–2787

Van den Berg MA, Steensma HY (1995) *ACS2*, a *Saccharomyces cerevisiae* gene encoding acetyl-coenzyme A synthetase, essential for growth on glucose. Eur J Biochem **231:** 704–713

Wei Y, Lin M, Oliver DJ, Schnable PS (2009) The roles of aldehyde dehydrogenases (ALDHs) in the PDH bypass of Arabidopsis. BMC Biochem **10:** 7

Williams M, Randall DD (1979) Pyruvate dehydrogenase complex from chloroplasts of *Pisum sativum* L. Plant Physiol **64:** 1099–1103

Wu X, Oh M-H, Schwarz EM, Larue CT, Sivaguru M, Imai BS, Yau PM, Ort DR, Huber SC (2011) Lysine acetylation is a widespread protein modification for diverse proteins in Arabidopsis. Plant Physiol **155:** 1769–1778

Young JD, Allen DK, Morgan JA (2014) Isotopomer measurement techniques in metabolic flux analysis II: Mass spectrometry. Methods Mol Biol **1083:** 85–108

Yu H, Du X, Zhang F, Zhang F, Hu Y, Liu S, Jiang X, Wang G, Liu D (2012) A mutation in the E2 subunit of the mitochondrial pyruvate dehydrogenase complex in *Arabidopsis* reduces plant organ size and enhances the accumulation of amino acids and intermediate products of the TCA cycle. Planta **236:** 387–399

Yuan J, Bennett BD, Rabinowitz JD (2008) Kinetic flux profiling for quantitation of cellular metabolic fluxes. Nat Protoc **3:** 1328–1340